JACS
JOURNAL OF THE AMERICAN CHEMICAL SOCIETY

Article

pubs.acs.org/JACS

Electron-Triggered Metamorphism in Porphyrin-Based Self-Assembled Coordination Polymers

Christophe Kahlfuss,[†] Sandrine Denis-Quanquin,[†] Nathalie Calin,[†] Elise Dumont,[†] Marco Garavelli,[†,§] Guy Royal,[‡] Saioa Cobo,[‡] Eric Saint-Aman,*[,‡] and Christophe Bucher*[,†]

[†]Univ Lyon, Ens de Lyon, CNRS UMR 5182, Université Claude Bernard Lyon 1, Laboratoire de Chimie, F69342 Lyon, France
[‡]Université Grenoble-Alpes, CNRS, Département de Chimie Moléculaire (UMR 5250), F38400 Grenoble, France
[§]Dipartimento di Chimica "G. Ciamician", Università di Bologna, V. F. Selmi 2, 40126 Bologna, Italy

Supporting Information

ABSTRACT: Viologen-centered electron transfer is used to trigger a complete dissociation of a porphyrin-based supramolecular architecture. In the oxidized state, self-assembly is induced by iterative association of individual porphyrin-based tectons. Dissociation of the self-assembled species is actuated upon changing the redox state of the bipyridium units involved in the tectons from their dicationic state to their radical cation state, the driving force of the disassembling process being the formation of an intramolecularly locked conformation partly stabilized by π-dimerization of both viologen cation radicals.

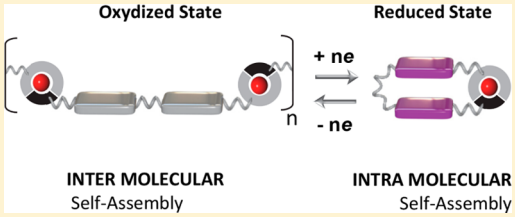

INTRODUCTION

Stimuli-responsive self-assembled molecular materials are currently subject to intense research activity.[1] This growing interest stems largely from the myriad of exciting applications envisioned for dynamic supramolecular assemblies, also known as dynamers,[2] in materials science, sensing, catalysis and electronics. Our own research activity over the past decade has mainly fallen within the scope of molecular metamorphism, a terminology borrowed from geologists that we use to picture the structural responses of molecules to external stimuli. The latter encompasses a wide range of well-defined and controllable molecular level motions achieved with synthetic molecules or interlocked molecules usually categorized in literature in two main groups according to trajectory and net produced task issues (molecular machines) or by default, in reference to the number of "stable" states involved in the system (molecular switches).[3] The prospect of extending these properties to the supramolecular level, i.e., to achieve for instance an electronic control over the organization or over the association/dissociation of molecular tectons within self-assembled materials[1,4] has recently led us to devise the concept of metal−organic self-assembled supramolecular system depicted in Figure 1.

The targeted monomer is a flexible molecule made out of three functional units. The key electron-responsive component, capable of actuating a large amplitude folding motion in response to an electron transfer (two electron reduction), is a bis-viologen hinge involving two 4,4′-bipyridinium units linked through a short, albeit flexible, covalent linker.[5] The two other key functional elements are the self-complementary recognition units introduced on either sides of the tecton. In the present work, this concept has been successfully implemented with a ligand and a coordination complex featuring a vacant and/or labile coordination site as the donor and acceptor units, respectively. One fundamental idea behind this triptych design is that the electrostatic repulsion between the two dicationic bipyridiniums involved in the central hinge prohibits the intramolecular recognition of the donor and acceptor in the

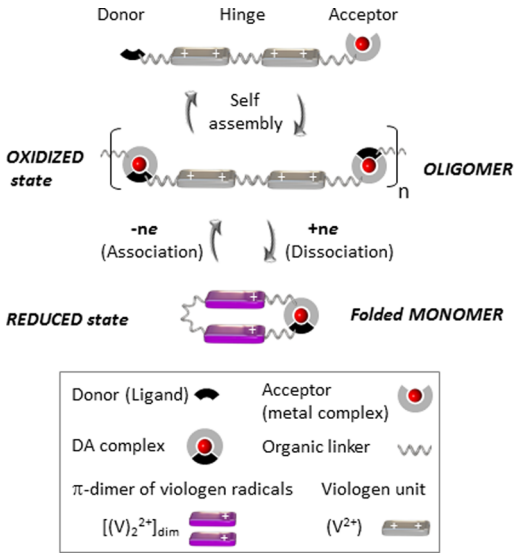

Figure 1. Concept of redox-switchable metal−organic self-assembled system.

Received: September 8, 2016
Published: October 21, 2016

DOI: 10.1021/jacs.6b09311
J. Am. Chem. Soc. 2016, 138, 15234−15242

initial state (+4 charge) and therefore enforces the formation of the supramolecular assembly depicted in Figure 1.

Another key feature is that its dissociation can be triggered electrochemically, upon simply changing the redox state of the viologen units from their dicationic state to their radical cation state,[6] the driving force of the targeted dissociation being the formation of an intramolecularly locked monomer stabilized by orthogonal interactions: (i) π-dimerization of both viologen cation radicals[5−7] and (ii) intramolecular recognition of the donor and acceptor moieties. According to this concept, we describe in the present article the first example of a porphyrin- and viologen-based redox-responsive tecton whose self-association properties can be controlled by electron transfer.

RESULTS AND DISCUSSION

Syntheses of the Redox Responsive Tectons. The monomer which has been designed to fulfill the structural requirements imposed by the general concept discussed above is the porphyrin-viologen compound **12**Zn^{4+} (Scheme 1). The latter features a zinc porphyrin and an imidazole ligand introduced at both ends of the molecule as the self-complementary acceptor and donor moieties, respectively.

The inner electron-responsive foldable hinge involves two dicationic 4,4′-bipyridinium units linked through a short and flexible propyl chain selected, in agreement with the $n = 3$ rule defined in the sixties by Hirayama,[8] for its ability to enable the targeted intramolecular folding motion.[7f,g,9] Another matter which required a careful optimization is the length of the rigid organic linkers introduced between the porphyrin acceptor and the first viologen unit and between the imidazole donor and the second viologen unit. Insertion of a phenylacetylene linkage on the porphyrin side and of a phenyldiacetylene linkage on the imidazole side have mainly been dictated by use of molecular models suggesting that such combination would allow the coordination of the imidazole ligand on the zinc atom in the folded π-dimerized conformation. The convergent synthesis of **12**Zn^{4+} proceeds in 18 steps through the asymmetric functionalization of the key intermediate **10**$^{4+}$ from two consecutive Zincke reactions[10] involving successively the aniline terminated building blocks **4**Zn and **9**. The porphyrin arm **4**Zn could be synthesized in three steps from the A_3B porphyrin intermediate **2** obtained in 24% yield as a result of the acid catalyzed condensation of 2,2′-dipyrrolylmethane with the 5,5′-dibutyryl-2,2′-(butane-1,1-diyl)bis(1H-pyrrole) **1**. Bromination of the only available *meso* position with *N*-bromosuccinimide, followed by metalation of the inner porphyrin with zinc acetate, led to **3**Zn, which was ultimately submitted to a Sonogashira coupling reaction involving ethynylaniline as a reactant to yield the targeted aniline appended porphyrin **4**Zn. The imidazole containing building block **9** has been synthesized in 7 steps from the commercially available methyl imidazole and 4-ethynylaniline, the key reaction being the palladium catalyzed Sonogashira cross-coupling between the known 2-ethynyl-1-methylimidazole **7** and the Boc-protected iodoethynylaniline **8**. The ultimate steps leading to the targeted tecton **12**Zn^{4+} involve submitting the activated bis-viologen precursor **10**$^{4+}$ to two consecutive Zincke reactions, first with the imidazole substituted aniline **9**, then with the porphyrin **4**Zn. Similar synthetic strategies have also been implemented to produce the reference compounds **6**Zn$(PF_6)_2$ and **13**$(PF_6)_2$ featuring a single viologen unit linked to a porphyrin ring or to an imidazole moiety, respectively.

Scheme 1[a]

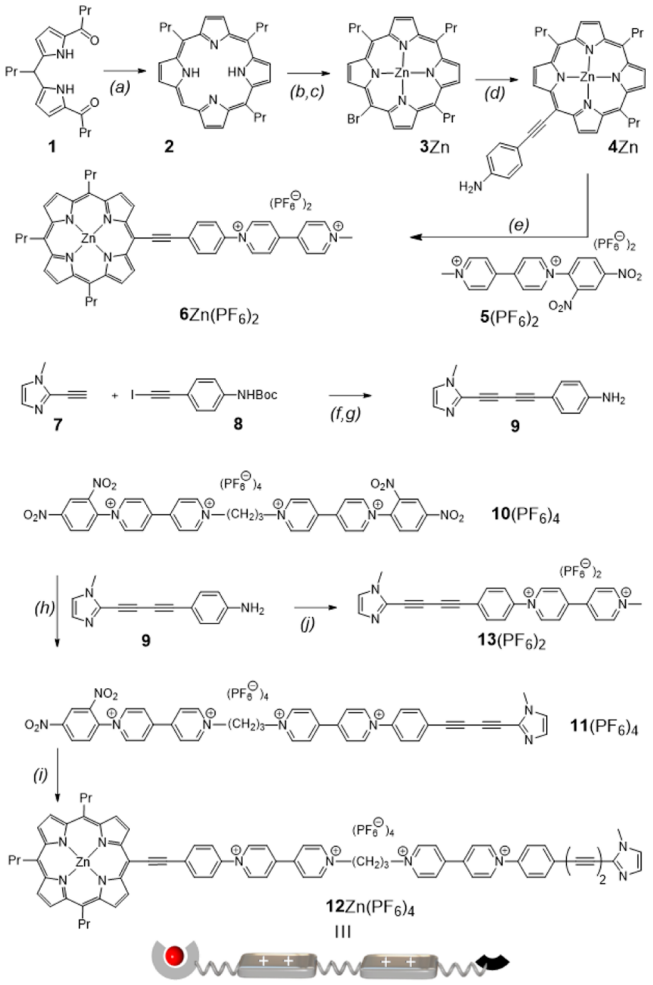

[a](a) (1) $NaBH_4$, MeOH/THF, rt 2 h; (2) 2,2′-dipyrromethane, CF_3CO_2H, DDQ, CH_3CN, r.t. 1 h, 24%. (b) NBS, $CHCl_3$, rt 30 min, 90%. (c) $Zn(OAc)_2$, MeOH/$CHCl_3$, rt 30 min, 92%. (d) 4-Ethynylaniline, $Pd(PPh_3)_2Cl_2$, CuI, THF/Et_3N, 50 °C, 18 h, 50%. (e) (1) TBACl, CH_3CN; (2) **4**Zn, EtOH/H_2O/THF, reflux, 18 h; (3) KPF_6, H_2O, 71%. (f) $Pd(PPh_3)_2Cl_2$, CuI, THF/Et_3N, 45 °C, 30 min, 40%. (g) CF_3CO_2H, CH_2Cl_2, rt 30 min, 90%. (h) **10**$(PF_6)_4$, EtOH/CH_3CN, reflux 5h, 61% (i) (1) TBACl, CH_3CN; (2) **4**Zn, EtOH/H_2O, THF, reflux 6 h; (3) KPF_6, H_2O, 30%. (j) **5**(PF6)$_2$, EtOH/CH_3CN, reflux 18 h, 58%.

Characterization of the Tetracationic Tecton 12Zn^{4+}. The reference species **6**Zn$(PF_6)_2$ and **13**$(PF_6)_2$, together with the title compound **12**Zn$(PF_6)_4$ have been fully characterized by NMR spectroscopy using 1D and 2D NMR experiments. One key feature of the ^{1}H NMR spectrum recorded for a 1 mM DMSO solution of **12**Zn$(PF_6)_4$ is that all the signals attributed to the viologen (V^{2+}), porphyrin (P) and imidazole (Im) moieties resonate at similar frequencies in the spectrum of **6**Zn^{2+}, **12**Zn^{4+} and **13**$^{4+}$ (Table 1), which implies that there is no significant association in such a competitive medium between the imidazole and porphyrin units of the triad **12**Zn^{4+}.

These findings thus led us to investigate the effects of solvent and concentration on its ability to self-assemble in solution. First evidence supporting the conclusion that the imidazole-viologen and the zinc porphyrin-viologen subunits can indeed self-associate in solution through the formation of an imidazole (N)-porphyrin (Zn) coordination bond have been obtained

DOI: 10.1021/jacs.6b09311
J. Am. Chem. Soc. 2016, 138, 15234−15242

Table 1. Selected ^{1}H NMR[d] Chemical Shifts Measured for $6Zn(PF_6)_2$, $13(PF_6)_2$, and $12Zn(PF_6)_4$[d]

	viologen	porphyrin	imidazole
$6Zn^{2+}$	9.83,[b] 9.32,[b] 8.99,[b] 8.89[b]	9.76,[b] 9.69,[b] 9.66,[b] 9.60[b]	
13^{2+}	9.15,[b] 8.89,[b] 8.58,[b] 8.45[b]		7.16,[a] 7.03[a]
$12Zn^{4+}$	9.87,[b] 9.74,[b] 9.47–9.42,[c] 9.05,[b] 9.00[b]	9.77,[b] 9.69,[b] 9.66,[b] 9.60[b]	7.41,[a] 6.99[a]

[d]DMSO-d_6 (1 mM, 400 MHz). a = singlet, b = doublet, c = multiplet.

with reference compounds, upon studying the intermolecular complexation of the donor 13^{2+} on the acceptor $6Zn^{2+}$.

Prior analysis involved monitoring the shift of the main porphyrin-based absorption bands in the spectrum of $6Zn^{2+}$ (0.1 mM) induced by a progressive addition of the donor 13^{2+}. Mixing both compounds turned out to have little effects when using solvents of large donicities[11] (DN) such as DMF (DN = 26.6 kcal mol^{-1}) and DMSO (DN = 29.8 kcal mol^{-1}). Use of a less competing solvent such as acetonitrile (DN = 14.1 kcal mol^{-1}) led conversely to the observation of a large bathochromic shift (~10 nm, see Figure 2A) of one porphyrin Q-band reached after addition of only 40 mol equiv of the donor 13^{2+}. Fitting of the 1/1 isotherm equation to the experimental data depicted in Figure 2B yielded a binding constant of about 360 M^{-1} which happens to fall significantly short of the average values measured in organic media with zinc porphyrins and nitrogen-based ligand.[12] The moderate affinity of the donor 13^{2+} for $6Zn^{2+}$measured in our experimental conditions can however be easily explained by the electron-withdrawing effect of the viologen units on the ligating ability of the imidazole donor combined with the use of a much more competitive solvent than those generally used with metalloporphyrins (acetonitrile versus chloroform or dichloromethane).

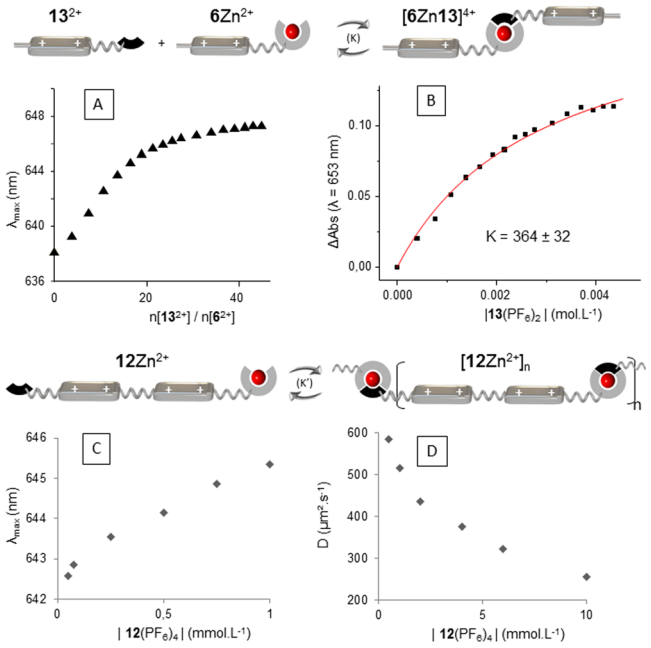

Figure 2. (A) Maximal absorption wavelength (λ_{max}) corresponding to a Q-band of $6Zn(PF_6)_2$ (10^{-4} M, CH_3CN) vs the ratio $n[13^{2+}]/n[6Zn^{2+}]$. (B) Curve fitting of the binding isotherm monitored at 653 nm (l = 1 mm). (C) Maximal absorption wavelength (λ_{max}) corresponding to a Q-band of $12Zn(PF_6)_4$ vs the concentration (CH_3CN). (D) Diffusion coefficient of $12Zn(PF_6)_4$ measured by DOSY NMR in CD_3CN vs the concentration.

Further evidence have been collected with the triad $12Zn^{4+}$, upon noticing that its NMR and UV–vis spectroscopic signatures exhibit concentration-dependent features (Figure 2C and D). For instance, the stepwise dilution of a 1 mM acetonitrile solution of $12Zn^{4+}$ down to 0.05 mM was found to result in a continuous hypsochromic shift of the porphyrins Q bands (Figure 2C), as expected due to the progressive dissociation of the self-assembled supramolecular architecture $[12Zn^{4+}]_n$ into the nonassociated monomer $12Zn^{4+}$ (Figure 2). Further insights into the impact of the concentration on the self-association processes involved in solution have been provided by diffusion ordered spectroscopy (DOSY) measurements giving access to the diffusion coefficient (D) characteristic of the molecular species present in solution. We found that the D value calculated for $12Zn^{4+}$ in deuterated acetonitrile goes down from 600 to 250 μm^2 s^{-1} as the concentration was increased from 0.5 to 10 mM. Here again, the observed drop in the D values supports the idea that a mixture of self-assembled species $[12Zn^{4+}]_n$ is formed in solution and that the size of the oligomers (n) mainly depends on the concentration of the monomer as well as on the nature of the solvent. The D values can potentially be used to estimate the number of monomers involved in the oligomer at a given concentration but this mathematical treatment can only be achieved upon making the assumption that the aggregates in solution have ideal geometries, typically either spherical or linear. Analyzing the D values collected with $[12Zn^{4+}]_n$ over the concentration range of 0.5–10 mM using these ideal geometrical pictures led to a variation of n values spanning from 4 to 12 (details are given in the Supporting Information (SI)). All the data collected in acetonitrile are thus in agreement with the formation of a mixture of oligomers $[12Zn^{4+}]_n$ whose length increases with concentration.

Characterization of the Bis(cation radical) $12Zn^{2(+\bullet)}$. Our next objective was to investigate the redox properties of $12Zn^{4+}$ and its ability to isomerize into a folded intramolecularly self-assembled structure in response to an electronic stimulus (Figure 3). Among all the possible techniques that have so far proved useful to reveal the existence of metamorphic processes involving π-dimerization, electrochemical methods might well stand as the most informative ones as they provide direct information about the fate of the electrogenerated radicals, about their stability as well as about the kinetics of the electron and chemical processes involved in the coupled mechanisms.[13]

The tecton $12Zn^{4+}$ as well as the reference compound $6Zn^{2+}$ have first been submitted to detailed electrochemical analyses in a DMF electrolyte, in which no supramolecular association occurs in the oxidized state over the investigated concentration range (5.10^{-4}–10^{-3} M). The voltamograms of both species exhibit one irreversible porphyrin-based oxidation and three consecutive reversible reduction waves observed between −400 and −1800 mV (Figure ESI 2). The two first reductions involve the viologen centers (V^{2+}) leading to the radical cation ($V^{+\bullet}$) then the neutral quinonic state (V^0), with the last reversible

DOI: 10.1021/jacs.6b09311
J. Am. Chem. Soc. 2016, 138, 15234–15242

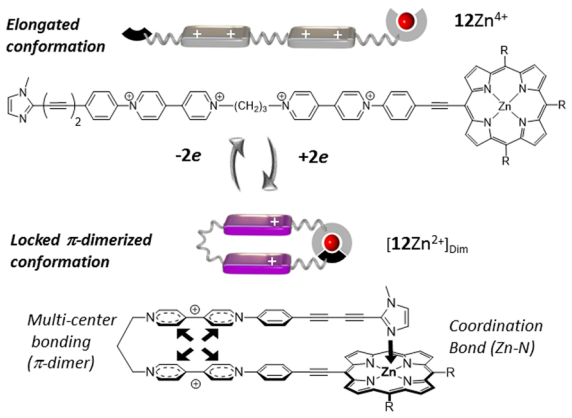

Figure 3. Schematic representation of the electron-triggered folding/unfolding processes.

wave centered at $E_{1/2}\sim -1700$ mV being attributed to the reduction of the porphyrin core ($P \rightarrow P^{\bullet -}$). The ability of the electrogenerated viologen cation radicals to self-assemble in solution to yield the intramolecular dimer $[\mathbf{12}Zn^{2+}]_{Dim}$ (Figure 3) can be readily judged from the values collected in Table 2 as

Table 2. Half-Wave Potentials ($E_{1/2}$), $\Delta E_p = E_{pa} - E_{pc}$, or Anodic Peak Potentials (E_{pa}) Measured for $\mathbf{12}Zn^{4+}$ and $\mathbf{6}Zn^{2+}$ (1 mM) in DMF + TBAP 0.1 M[a]

	E_{pa} [P→P$^{+\bullet}$]	$E_{1/2}$ [V^{2+}→V$^{+\bullet}$]	$E_{1/2}$ [V$^{+\bullet}$→V^{0}]	$E_{1/2}$ [P→P$^{\bullet -}$]
$\mathbf{12}Zn^{4+}$	377	−479 (47)	−1096 (102)	−1711 (65)
$\mathbf{6}Zn^{2+}$	348	−687 (58)	−998 (59)	−1725 (62)

[a]Vitreous carbon WE, Φ = 3 mm, ν = 0.5 V s^{-1}, E vs Ag/Ag^{+} 10^{-2} M). "P" and "V" stand for "porphyrin" and "viologen".

well as from the CV curves shown in Figure 4A. The latter show that *i*) the stability domain of the V$^{+\bullet}$ state is much larger for $\mathbf{12}Zn^{4+}$ (Figure 4, $[E_{1/2}]_1^* - [E_{1/2}]_2^* = 617$ mV) than for the reference compound $\mathbf{6}Zn^{2+}$ (Figure 4, $[E_{1/2}]_1^{\#} - [E_{1/2}]_2^{\#} = 311$ mV) and that *ii*) the peak to peak potential shift (ΔE_p) measured on the first reduction wave is far lower for $\mathbf{12}Zn^{4+}$ than for $\mathbf{6}Zn^{2+}$ (30 vs 58 mV measured at 0.02 V s^{-1}). These fundamental differences found between the mono- and bis-viologen derivatives are unambiguously imputable to the extensive stabilization of the V$^{+\bullet}$ units in the π-dimer $[\mathbf{12}Zn^{2+}]_{Dim}$ (Figure 3 and Figure ESI 1). The occurrence of an isomerization step (folding) coupled to the electron transfer (1e/viologen) has thus two main effects which can be considered as the hallmarks of π-dimerizations involving viologen radicals:[5] (i) it facilitates the reduction of the viologen centers $E_{1/2}[V^{2+} \rightarrow V^{+\bullet}]_{12Zn} \gg E_{1/2}[V^{2+} \rightarrow V^{+\bullet}]_{6Zn}$ and (ii) it lowers the ΔE_p value far below the theoretical 58 mV shift expected for a standard Nernstian process $\Delta E_p[V^{2+} \rightarrow V^{+\bullet}]_{6Zn} \gg \Delta E_p[V^{2+} \rightarrow V^{+\bullet}]_{12Zn}$ (Table 2).

Another key objective was to reveal the intramolecular nature of the dimerization process, as anticipated in the formation of $[\mathbf{12}Zn^{2+}]_{Dim}$ from $\mathbf{12}Zn^{4+}$ (Figure 3). The latter was established upon showing that key experimental data such as (i) the absorption intensity at 940 nm evolves linearly with the concentration of $[\mathbf{12}Zn^{2+}]_{Dim}$ (Figure ESI 5) and (ii) the peak-potential values and the associated peak to peak separation (ΔE_p) do no vary over the accessible concentration range (Figure 4C) or that the reference compound $\mathbf{6}Zn^{2+}$ does not dimerize in the same experimental conditions. Further insights into the relative importance of the kinetics of the electrochemical and chemical steps involved in the intramolecular dimerization have been obtained upon studying the electrochemical signature of $\mathbf{12}Zn^{4+}$and $\mathbf{6}Zn^{2+}$ at different scan rates.

As seen on the data plotted in Figure 4B, we found that the time scale of the CV measurement has no influence on the ΔE_p value measured for the reference $\mathbf{6}Zn^{2+}$ which happens to be invariant (~60 mV) over the entire scan rate range. A fully different behavior was observed with the dimerizable species

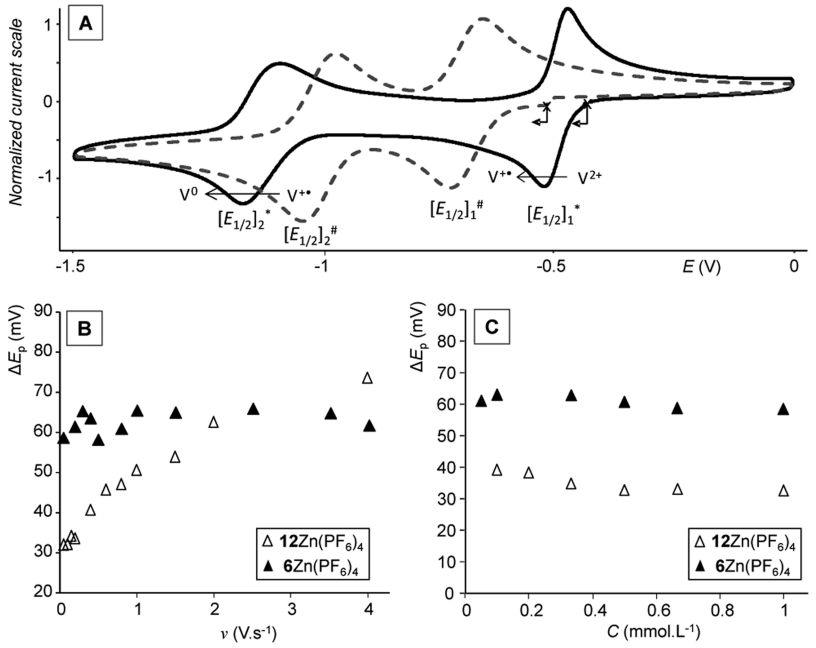

Figure 4. (A) Voltamograms of $\mathbf{12}Zn(PF_6)_4$ (full line, 0.2 mM, and $\mathbf{6}Zn(PF_6)_2$ (dashed line, 0.25 mM) (ν = 100 mV s^{-1}). (B) Peak to peak potential (ΔE_p) measured for $\mathbf{12}Zn(PF_6)_4$ and $\mathbf{6}Zn(PF_6)_2$ at various scan rates (1 mM). (C) Peak to peak potential (ΔE_p) measured for $\mathbf{12}Zn(PF_6)_4$ and $\mathbf{6}Zn(PF_6)_2$ at various concentrations (ν = 0.1 V s^{-1}). VC, Φ = 3 mm, DMF + TBAP 0.1 M, E vs Ag/Ag^{+} 10^{-2} M.

DOI: 10.1021/jacs.6b09311
J. Am. Chem. Soc. 2016, 138, 15234−15242

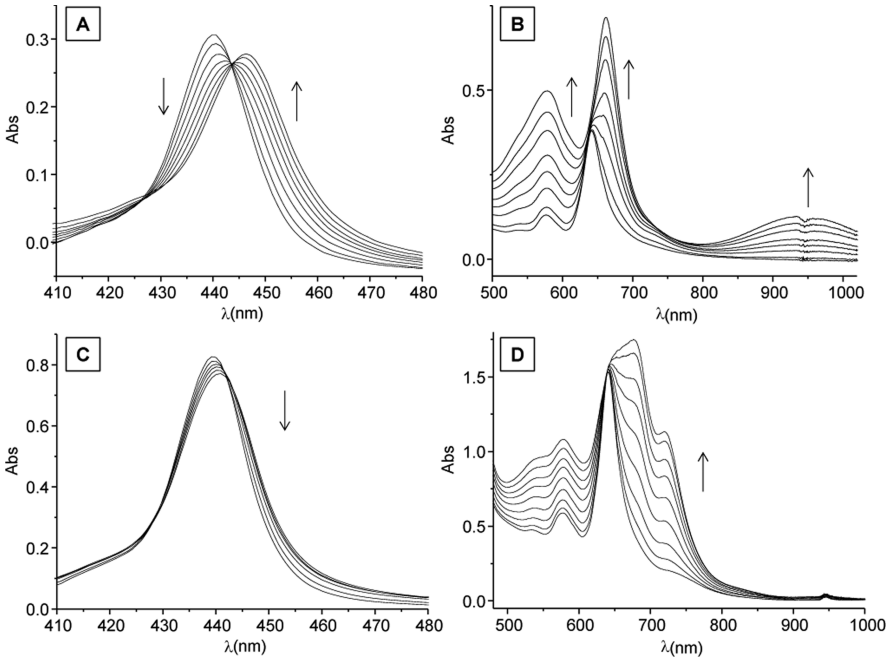

Figure 5. UV/vis spectra recorded during the exhaustive electrolysis (one electron per viologen) of **12**Zn$(PF_6)_4$ at (A) 2×10^{-5} mol L^{-1} and (B) 2×10^{-4} mol L^{-1} and of **6**Zn$(PF_6)_2$ at (C) 2×10^{-5} mol L^{-1} and (D) 4×10^{-4} mol L^{-1} in DMF (0.1 M TBAP) (working electrode: Pt, $E_{app} = -0.8$ V, 10 mL, $l = 1$ mm, $t \approx 30$ min).

12Zn^{4+}, with ΔE_p values found to be ranging from 30 mV at low rates ($\nu = 0.02$ V s^{-1}) up to 75 mV measured at 4 V s^{-1} (Figure 4B). The stability of the data measured for the reference compound **6**Zn^{2+} from 20 mV s^{-1} to 4 V s^{-1} ($\Delta E_p \sim$ 60 mV) thus supports the conclusion that the changes observed with the bis-viologen compound **12**Zn^{4+} are not due to a kinetic limitation of the electron transfer centered on the viologens ($V^{2+}/V^{+\bullet}$) but rather to the relatively slow kinetics of the coupled chemical steps involving fully and partially reduced species, namely the π-dimerization of the doubly reduced species **12**$Zn^{2(+\bullet)} \leftrightarrow$ [**12**Zn^{2+}]$_{Dim}$, and the disproportionation of the one electron reduced species **12**$Zn^{3+\bullet}$ into **12**$Zn^{2(+\bullet)}$ and **12**Zn^{4+}.

The folding motion yielding the locked dimer [**12**Zn^{2+}]$_{Dim}$ (Figure 3) has been further investigated by spectroelectrochemistry, which involved regularly recording absorption spectra over time during the potentiostatic reduction of **12**Zn^{4+} or **6**Zn^{2+}. The bulk electrolysis (1e/viologen) of the reference compound **6**Zn^{2+} carried out at 2.10^{-5} or 4.10^{-4} M in DMF at a platinum electrode only led to a slight broadening of the porphyrin-based Soret band centered at 339 nm which came along with a weak bathochromic shift, of less than 1 nm, of its maximum wavelength (Figure 5C).

In the red region of the electromagnetic spectrum, formation of the one electron reduced species **6**$Zn^{+\bullet}$ is revealed through the growth of a series of bands, centered at 578 (27000 L mol^{-1} cm^{-1}), 676 (43800 L mol^{-1} cm^{-1}) and 719 nm (28300 L mol^{-1} cm^{-1}) (Figure 5D), attributed to the $V^{+\bullet}$ unit whose signature appears moderately affected by the porphyrin substituent.

The same analyses carried out on DMF solutions of **12**Zn^{4+} led to a completely different picture, the main features of the absorption spectrum recorded after addition of two electrons (1e/viologen) being the broad absorption band centered at 940 nm (6300 L mol^{-1} cm^{-1}) and the 6 nm shift experienced by the Soret band (Figure 5A and B). In the 500−1100 nm region, the progressive accumulation of the doubly reduced species leads to the progressive growth of bands centered at $\lambda_{max} = 578$ (25000 L mol^{-1} cm^{-1}), 662 (35800 L mol^{-1} cm^{-1}), and 940 nm (6300 L mol^{-1} cm^{-1}), which are the distinctive attribute of π-dimers involving viologen radicals.[5] In the blue part of the electromagnetic spectra (Figure 5A), reduction of the viologens comes along with a progressive disappearance of the initial Soret band at the expense of a new band appearing at lower energy, an evolution which is often observed as the result of the coordination of exogenous ligands onto the available axial binding site of metalloporphyrins.[12c,14] The modification seen in the 400−1100 nm range upon reducing the viologen units are thus fully compatible with the formation of the folded structure [**12**Zn^{2+}]$_{Dim}$, both the coordination of the imidazole unit and the formation of the π-dimer complex being unambiguously demonstrated by the data depicted in Figure 5.

ESR spectroscopy data have also been found to support the same conclusions. The X-band spectrum of the one electron reduced species **6**$Zn^{+\bullet}$, recorded at room temperature on a sample previously submitted to an exhaustive one-electron electrolysis, shows the expected intense and broad signal attributed to the presence of a single electron delocalized over the viologen unit (Figure ESI 3).

The two-electron reduced sample of **12**Zn^{4+} has conversely been found to be fully ESR silent (Figure ESI 3) as a consequence of the tight coupling and electron pairing occurring between both $V^{+\bullet}$ units within the folded structure [**12**Zn^{2+}]$_{Dim}$. It should be mentioned that the complete absence of residual paramagnetic signal in the spectrum of [**12**Zn^{2+}]$_{Dim}$ stands in sharp contrast to what is systematically observed in solution with flexible bis-viologen derivatives due to the fact that the diamagnetic π-dimerized complex and the paramagnetic open bis-radicals are both involved in an equilibrium which happens to be more or less displaced toward one species or the other depending on the stabilization energy associated with the dimerization.[7] These unprecedented results thus led us to propose that the coordination bond established between the

DOI: 10.1021/jacs.6b09311
J. Am. Chem. Soc. 2016, 138, 15234−15242

imidazole ring and the zinc atom leads to a locked macrocyclic structure providing both a kinetic and thermodynamic stabilization to the dimer $[\mathbf{12}Zn^{2+}]_{Dim}$.

The fully reversible folding—unfolding process $\mathbf{12}Zn^{4+} \leftrightarrow [\mathbf{12}Zn^{2+}]_{Dim}$ triggered by electron transfer can be analyzed based on density functional theory (DFT) calculations and energy decomposition analysis.[15] The range-separated hybrid functional CAM-B3LYP-D3BJ was used alongside with the 6-311G(d,p) basis set for all atoms, except for the zinc dication for which the LANL2DZ pseudopotential[16] was used. Solvation by acetonitrile was taken into account through a polarizable continuum model.[17]

The energetic diagram depicted in Figure 6 shows the relative energies calculated between the folded and elongated

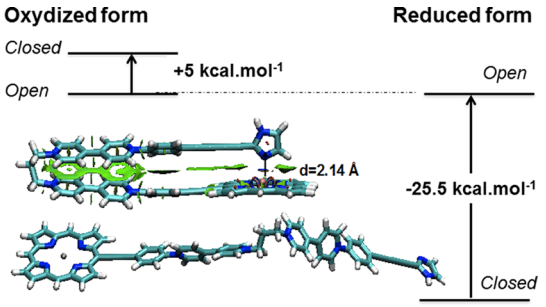

Figure 6. Energetic scheme (in kcal mol^{-1}) and cartoon representations for $[\mathbf{12}Zn^{4+}]_{open}$ and $[\mathbf{12}Zn^{2+}]_{Dim}$ comparing the energy between folded and extended conformations.

conformers in their reduced ($[\mathbf{12}Zn^{2+}]_{Dim}$ vs $[\mathbf{12}Zn^{2(+\bullet)}]_{open}$) and oxidized ($[\mathbf{12}Zn^{4+}]_{folded}$ vs $[\mathbf{12}Zn^{4+}]_{open}$) forms. The open conformation found as the most stable state for the tetracationic, i.e. nonreduced, compound is mainly imposed by the electrostatic repulsive forces occurring between both viologens. As expected from the experimental data discussed above, the largest stabilization energy, of about −25.5 kcal mol^{-1}, is obtained at the reduced state for the intramolecularly dimerized complex $[\mathbf{12}Zn^{2+}]_{Dim}$. The extent of stabilization within the folded structure results from the additive contributions of the N···Zn bond, accounting for −16.0 kcal mol^{-1} (as evaluated along a relaxed scan), and of the multicenter bonding involved in the π-dimer. In the folded conformers, a NCI (noncovalent interaction) analysis[18] has been carried out to visualize the dispersive interactions taking place between the two arms (green isodensity region in Figure 6). As can be seen on the model depicted in Figure 6, the folded conformation of $[\mathbf{12}Zn^{2+}]_{Dim}$. is locked by a nitrogen-(Im)−zinc coordination bond of about 2.14 Å, which happens to be only 0.1 Å longer than the one estimated on the reference intermolecular complex formed between $\mathbf{6}Zn^{2+}$ and $\mathbf{13}^{2+}$ (see Figure ESI 4). Our calculations and minimized structures also served to validate the choice of the propyl (central hinge), phenylacetylene (porphyrin arm) and phenyldiacetylene (imidazole arm) linkages introduced in $\mathbf{12}Zn^{4+}$ as they allow a perfect positioning of the imidazole ligand on top of the zinc atom in the folded conformation. In support of this statement, we found that shortening or increasing the number of carbon atoms (n) involved in the central alkyl chain connecting both bipyridiniums leads to much weaker global stabilization energies of −16.3 (n = 2) and −11.8 (n = 4) kcal mol^{-1} (see Figure ESI 4).

The higher stabilization of −25.5 kcal mol^{-1} found with the propyl linker (n = 3) thus clearly arises from a near-ideal stacking of both viologen cation radicals. The back oxidation of each viologen cation radical involved in the dimer ($V^{+\bullet} \rightarrow V^{2+}$) triggers the unfolding process $[\mathbf{12}Zn^{2+}]_{Dim} \rightarrow [\mathbf{12}Zn^{4+}]_{open}$, its driving force being the electrostatic repulsion between both dicationic units (see energy decomposition analysis in Table ESI 1).

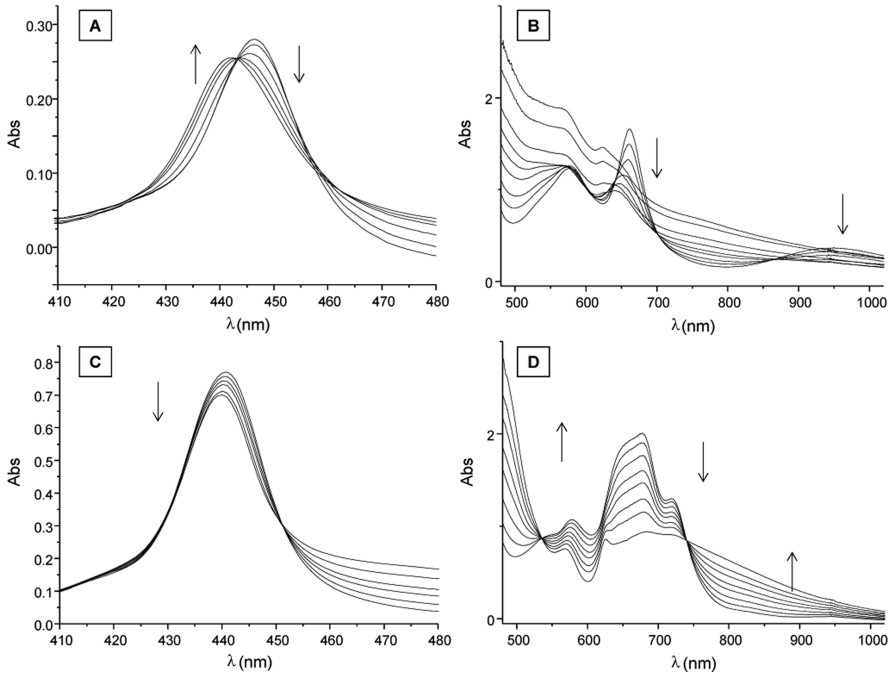

Figure 7. UV/vis spectra recorded during the exhaustive electrolysis (one electron per viologen) of $\mathbf{12}Zn^{2(+\bullet)}$ at (A) 2.10^{-5} mol L^{-1} and (B) 5.10^{-4} mol L^{-1} and of $\mathbf{6}Zn^{(+\bullet)}$ at (C) 2.10^{-5} mol L^{-1} and (D) 5.10^{-4} mol L^{-1} in DMF (0.1 M TBAP) (working electrode: Pt, E_{app} = −1.4 V, 10 mL, l = 1 mm, $t \approx 30$ min).

DOI: 10.1021/jacs.6b09311
J. Am. Chem. Soc. 2016, 138, 15234−15242

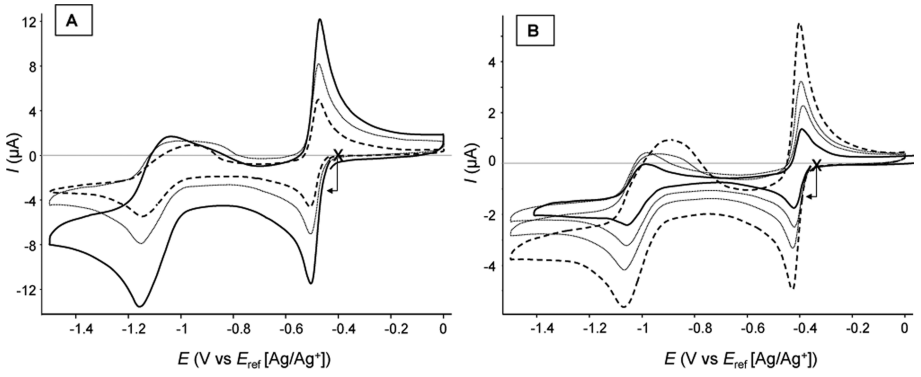

Figure 8. Voltametric curves recorded for $\mathbf{12}Zn(PF_6)_4$ (A) at various scan rates, from ν = 20 mV s^{-1} (dashed line) to 100 mV s^{-1} (full line) (1 mM), and (B) at various concentrations, from C = 1 mM (dashed line) to C = 0.33 mM (full line) (ν = 20 mV s^{-1}). (DMF + TBAP 0.1 M, vitreous carbon working electrode, Ø = 3 mm, E vs Ag/Ag^+ 10^{-2} M).

Characterization of the Neutral Quinonic State $\mathbf{12}Zn^0$. All the experimental evidence presented above fully support the conclusion that $\mathbf{12}Zn^{4+}$ self-assembles in CH_3CN and that the reduction of both viologens leads to an intramolecularly locked π-dimer prohibiting self-assembly. We then turned our attention to the tetra-reduced species $\mathbf{12}Zn^0$, wherein both viologens have been fully reduced up to their neutral quinonic states. We reckoned that further reduction of both cation radicals in $[\mathbf{12}Zn^{2+}]_{Dim}$ would be an alternative way (i) to trigger the dissociation of the intramolecular π-dimer $[\mathbf{12}Zn^{2+}]_{Dim}$ and (ii) to produce an electron rich neutral species with improved self-assembling properties due to the enhancement of the electron density on the imidazole ring, an assumption which has been moreover confirmed by computational analyses revealing that the electron population on the nitrogen atom of the imidazole ring increases from 0.96 in the tetracationic derivative $\mathbf{13}^{4+}$ to 1.93 in the doubly reduced species $\mathbf{13}^0$.

Further experiments aiming at evaluating the effects of the second viologen-centered reduction on the spectroscopic signature of the metalloporphyrin unit have been carried out with the reference compound $\mathbf{6}Zn^{2+}$. The modifications observed in the so-called Soret and Q bands regions during the bulk one-electron electrochemical reduction of DMF electrolytic solutions of $\mathbf{6}Zn^{+\bullet}$ at 5.10^{-4} M or 2.10^{-5} M are depicted in Figure 7D and C, respectively. The latter reveals that the reduction process has a limited influence on the Soret band which undergoes a very small hypsochromic shift, of about 1 nm, coming along with a significant loss of its intensity (~10%). The one-electron reduction leads expectedly to more important changes in the Q-band region, the most notable one being the collapse of the main signal centered at 680 nm attributed to the viologen cation radical. Another key feature observed in both regions is the presence of well-defined isosbestic points suggesting that the reduction process is a simple equilibrium involving only two species, namely $\mathbf{6}Zn^{+\bullet}$ and $\mathbf{6}Zn^0$.

Similar analyses have then been conducted on the bis-viologen species $\mathbf{12}Zn^{4+}$. We found that the two-electron reduction (1e/viologen) of a diluted DMF solution of $[\mathbf{12}Zn^{2+}]_{Dim}$ (0.02 mM) leads to a much larger hypsochromic shift of the Soret band ($\Delta\lambda_{max}$ = 3 nm) proceeding here again through a clear isosbestic point at 443 nm (Figure 7A). These data taken together with those collected in the same conditions with the reference compound $\mathbf{6}Zn^{+\bullet}$ led us to the conclusion that reducing $[\mathbf{12}Zn^{2+}]_{Dim}$ up to the V^0 state results in the disruption of the imidazole-Zinc coordination bond as well as in the dissociation of the intramolecular π-dimer, the latter being also supported by the disappearance of the broad absorption band centered at 900 nm (Figure 7B). The observation of a well-defined isosbestic point in the series of spectra collected in Figure 7A also reveals that the fully reduced tectons $[\mathbf{12}Zn^0]_{open}$, featuring an elongated conformation, do not self-assemble in these conditions (0.02 mM in DMF). The first hint of the key role of concentration on the self-association capability of $[\mathbf{12}Zn^0]_{open}$ came from the spectroelectrochemical data depicted in Figure 7B. The modifications observed in the Q-band region as the bulk reduction was carried out on a 0.5 mM DMF solution of $[\mathbf{12}Zn^{2+}]_{Dim}$ indeed not only bring to light the dissociation of the dimer through the disappearance of the diagnostic signature centered at λ_{max} = 940 nm, they also support the involvement of multiple equilibria, most notably from the modifications observed by the end of the experiment (Figure 7B). In the first stage of the electrolysis, between 0 and ~1 exchanged electron/molecule, the intensity of the main signals centered at 578, 662, and 940 nm follows a continuous decay proceeding through well-defined isosbestic points. Further reduction of the solution, up to an exchanged charge of two electrons/molecule, conversely leads to a continuous increase of the absorption on the whole frequency range proceeding without precipitation nor adsorption at the electrode surface. These changes and the ill-defined spectra recorded after two-electron reduction of $[\mathbf{12}Zn^{2+}]_{Dim}$ are thus fully compatible with the formation of self-assembled species involving $[\mathbf{12}Zn^0]_{open}$.

These conclusions are also supported by CV data showing that both concentration and scan rate influence the self-assembling of the fully reduced species $[\mathbf{12}Zn^0]_{open}$. The CV curves depicted in Figure 8, recorded on a 1 mM DMF solution of $\mathbf{12}Zn^{4+}$, show that the time scale of the experiment has an influence on the reversible character of the second reduction wave. At ν = 100 mV s^{-1} or higher, the latter appears as a well-defined "reversible" wave featuring a ΔE_p value of about 107 mV (The CV wave recorded at 0.5 V s^{-1} is shown in Figure ESI 2).

Increasing the time scale of the experiment, upon scanning the electrode potential at 20 mV s^{-1}, is found to affect the shape of the back oxidation wave ($[\mathbf{12}Zn^0]_{open} \rightarrow [\mathbf{12}Zn^{2+}]_{Dim}$) which appears much broader and significantly shifted to more positive potential values (ΔE_p = +190 mV). These results are consistent with the idea that the time scale at 20 mV s^{-1} is large enough to enable the formation of a mixture of self-assembled

DOI: 10.1021/jacs.6b09311
J. Am. Chem. Soc. 2016, 138, 15234−15242

supramolecular species ($n\mathbf{12}Zn^{0} \leftrightarrow [\mathbf{12}Zn^{0}]_n$) whose reoxidation appears as a broad and positively shifted wave. The fact that the oxidation of the viologen units become harder in $[\mathbf{12}Zn^{0}]_n$ can be explained by the stabilization[19] of the V^0 states in the oligomers which also acts as an impediment to the back formation of the intramolecular dimer $[\mathbf{12}Zn^{2+}]_{Dim}$. At higher scan rates, the electrogenerated species $[\mathbf{12}Zn^{0}]_{open}$ has no time to self-assemble and the reduction wave appears as a reversible process. Varying the concentration of samples submitted to CV measurements carried out at a constant scan rate (20 mV s^{-1}) was also found to affect the shape of the second reduction wave. The curves collected in Figure 8B reveal that the progressive decrease of the concentration within the 10^{-3} to 3×10^{-4} M range allows to convert the broad, ill-defined "irreversible" signature (ΔE_p = 190 mV) into a well-defined wave featuring all the characteristics of a reversible system (ΔE_p = 80 mV). All these electrochemical and spectroscopic data thus bring to light the existence of self-assembling equilibria involving the fully reduced species $[\mathbf{12}Zn^{0}]_{open}$ to form a mixture of oligomers ($[\mathbf{12}Zn^{0}]_n$) whose length depends on the concentration and time scale of the experiments. The schematic drawings shown in Figure 9 summarize the electrochemical (E) and chemical

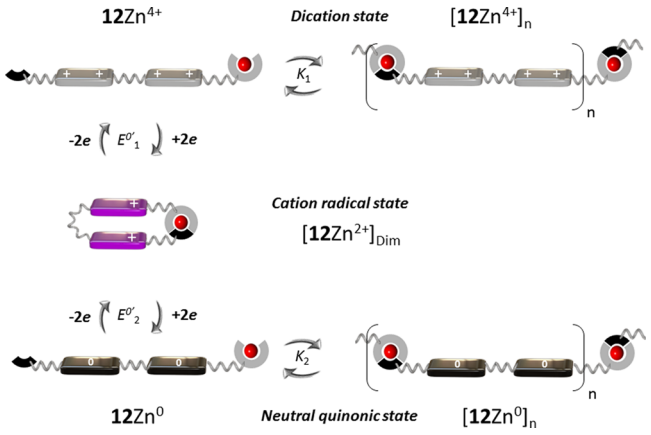

Figure 9. Schematic representation of the electron-triggered folding/unfolding processes involving the dicationic, cation radical, and neutral states of the viologen units.

equilibria (C) involved in solution as a function of the oxidation state of the viologen units (dicationic, cation radical and neutral).

CONCLUSION

In summary, we have devised a trifunctional molecular tecton whose self-assembling properties can be reversibly switched on and off upon controlling the redox state of a central bis(bipyridinium) hinge. In its tetracationic state, the iterative association of individual porphyrin-based tectons leads to the formation of soluble coordination oligomers whose size increases with concentration. Our investigations have revealed that self-assembly occurs in acetonitrile both for the tetracationic $\mathbf{12}Zn^{4+}$and for the fully reduced neutral species $\mathbf{12}Zn^{0}$. Another key finding is that the two-electron reduction of the viologen centers up to neutral V^0 state enhances the self-assembling capability of the tectons, as proved by the fact that $\mathbf{12}Zn^{4+}$ does not oligomerize in DMF at 1 mM whereas $\mathbf{12}Zn^{0}$ does.

Dissociation of the self-assembled coordination polymer $[\mathbf{12}Zn^{4+}]_n$ or $[\mathbf{12}Zn^{0}]_n$ is actuated upon changing the redox state of the bipyridium units involved in the tectons from their dicationic (V^{2+}) or neutral states (V^0) to their radical cation state ($V^{+\bullet}$), with the driving force of the disassembling process being the formation of an intramolecularly locked conformation partly stabilized by π-dimerization of both viologen cation radicals.

This novel concept of electron-switchable molecule not only opens up new perspectives in materials science, most notably for the development of adaptive supramolecular polymers that could respond to well-defined and controlled external stimuli by changes in structure and function. It also offers exciting opportunities in electrocatalysis and in analytic science, with the possibility to access functional molecular materials featuring porphyrin- and/or viologen-based redox-controllable electrocatalytic and transport/recognition properties.

ASSOCIATED CONTENT

Supporting Information

The Supporting Information is available free of charge on the ACS Publications website at DOI: 10.1021/jacs.6b09311.

Crystal data for **8** (CIF)
Crystal data for **9** (CIF)
Crystal data for $\mathbf{13}(H_2O)_2Cl_2$ (CIF)
Experimental details and characterization data (PDF)

AUTHOR INFORMATION

Corresponding Authors

*eric.saint-aman@ujf-grenoble.fr
*christophe.bucher@ens-lyon.fr

Notes

The authors declare no competing financial interest.

ACKNOWLEDGMENTS

This article is dedicated to Dr. Jean-Pierre Sauvage in recognition of his major and inspiring influence on our thinking and knowledge. This work was supported by the "Agence National de la Recherche" (ANR-12-BS07-0014-01) and by the Labex Arcane (ANR-11-LABX-0003-01).

REFERENCES

(1) (a) Ma, X.; Tian, H. *Acc. Chem. Res.* **2014**, *47*, 1971−1981. (b) Wang, A.; Shi, W.; Huang, J.; Yan, Y. *Soft Matter* **2016**, *12*, 337−357.

(2) Roy, N.; Bruchmann, B.; Lehn, J.-M. *Chem. Soc. Rev.* **2015**, *44*, 3786−3807.

(3) (a) Le Poul, N.; Colasson, B. *ChemElectroChem* **2015**, *2*, 475−496. (b) Kay, E. R.; Leigh, D. A. *Angew. Chem., Int. Ed.* **2015**, *54*, 10080−10088. (c) Fahrenbach, A. C.; Warren, S. C.; Incorvati, J. T.; Avestro, A.-J.; Barnes, J. C.; Stoddart, J. F.; Grzybowski, B. A. *Adv. Mater.* **2013**, *25*, 331−348. (d) Sauvage, J.-P.; Collin, J.-P.; Durot, S.; Frey, J.; Heitz, V.; Sour, A.; Tock, C. *C. R. Chim.* **2010**, *13*, 315−328. (e) Zhang, G.; Zhang, D.; Zhu, D. In *Electrochemistry of Functional Supramolecular Systems*; Ceroni, P., Credi, A., Venturi, M., Eds.; John Wiley & sons, Inc.: Hoboken, NJ, 2010.

(4) (a) Steed, J. W. *Chem. Commun.* **2011**, *47*, 1379−1383. (b) Kim, D. S.; Chang, J.; Leem, S.; Park, J. S.; Thordarson, P.; Sessler, J. L. *J. Am. Chem. Soc.* **2015**, *137*, 16038−16042. (c) Dong, S.; Gao, L.; Li, J.; Xu, D.; Zhou, Q. *Polym. Chem.* **2013**, *4*, 3968−3973. (d) López, J. L.; Pérez, E. M.; Viruela, P. M.; Viruela, R.; Orti, E.; Martín, N. *Org. Lett.* **2009**, *11*, 4524−4527. (e) Shibata, M.; Tanaka, S.; Ikeda, T.; Shinkai, S.; Kaneko, K.; Ogi, S.; Takeuchi, M. *Angew. Chem., Int. Ed.* **2013**, *52*, 397−400. (f) Benyettou, F.; Zheng, X.; Elacqua, E.; Wang, Y.; Dalvand, P.; Asfari, Z.; Olsen, J.-C.; Han, D. S.; Saleh, N. i.; Elhabiri, M.; Weck, M.; Trabolsi, A. *Langmuir* **2016**, *32*, 7144−7150. (g) Chen,

DOI: 10.1021/jacs.6b09311
J. Am. Chem. Soc. 2016, 138, 15234−15242

L.; Wang, H.; Zhang, D.-W.; Zhou, Y.; Li, Z.-T. *Angew. Chem., Int. Ed.* **2015**, *54*, 4028−4031. (h) McConnell, A. J.; Wood, C. S.; Neelakandan, P. P.; Nitschke, J. R. *Chem. Rev.* **2015**, *115*, 7729−7793.
(5) Kahlfuss, C.; Saint-Aman, E.; Bucher, C. In *Organic Redox Systems: Synthesis, Properties, and Applications*; Nishinaga, T., Ed.; John Wiley and Sons: New York, 2016.
(6) (a) Zhang, D.-W.; Tian, J.; Chen, L.; Zhang, L.; Li, Z.-T. *Chem. - Asian J.* **2015**, *10*, 56−58. (b) Spruell, J. M. *Pure Appl. Chem.* **2010**, *82*, 2281−2294.
(7) (a) Kahlfuss, C.; Métay, E.; Duclos, M.-C.; Lemaire, M.; Milet, A.; Saint-Aman, E.; Bucher, C. *Chem. - Eur. J.* **2015**, *21*, 2090−2106. (b) Kahlfuss, C.; Métay, E.; Duclos, M.-C.; Lemaire, M.; Oltean, M.; Milet, A.; Saint-Aman, E.; Bucher, C. *C. R. Chim.* **2014**, *17*, 505−511. (c) Kahlfuss, C.; Milet, A.; Wytko, J. A.; Weiss, J.; Saint-Aman, E.; Bucher, C. *Org. Lett.* **2015**, *17*, 4058−4061. (d) Iordache, A.; Kannappan, R.; Métay, E.; Duclos, M.-C.; Pellet-Rostaing, S.; Lemaire, M.; Milet, A.; Saint-Aman, E.; Bucher, C. *Org. Biomol. Chem.* **2013**, *11*, 4383−4389. (e) Iordache, A.; Oltean, M.; Milet, A.; Thomas, F.; Saint-Aman, E.; Bucher, C. *J. Am. Chem. Soc.* **2012**, *134*, 2653−2671. (f) Iordache, A.; Retegan, M.; Thomas, F.; Royal, G.; Saint-Aman, E.; Bucher, C. *Chem. - Eur. J.* **2012**, *18*, 7648−7653. (g) Kannappan, R.; Bucher, C.; Saint-Aman, E.; Moutet, J.-C.; Milet, A.; Oltean, M.; Métay, E.; Pellet-Rostaing, S.; Lemaire, M.; Chaix, C. *New J. Chem.* **2010**, *34*, 1373−1386. (h) Iehl, J.; Frasconi, M.; Jacquot de Rouville, H.-P.; Renaud, N.; Dyar, S. M.; Strutt, N. L.; Carmieli, R.; Wasielewski, M. R.; Ratner, M. A.; Nierengarten, J.-F.; Stoddart, J. F. *Chem. Sci.* **2013**, *4*, 1462−1469. (i) Nchimi-Nono, K.; Dalvand, P.; Wadhwa, K.; Nuryyeva, S.; Alneyadi, S.; Prakasam, T.; Fahrenbach, A. C.; Olsen, J.-C.; Asfari, Z.; Platas-Iglesias, C.; Elhabiri, M.; Trabolsi, A. *Chem. - Eur. J.* **2014**, *20*, 7334−7444. (j) Wang, Y.; Frasconi, M.; Liu, W.-G.; Sun, J.; Wu, Y.; Nassar, M. S.; Botros, Y. Y.; Goddard, W. A., III; Wasielewski, M. R.; Stoddart, J. F. *ACS Cent. Sci.* **2016**, *2*, 89−98. (k) Gao, C.; Silvi, S.; Ma, X.; Tian, H.; Credi, A.; Venturi, M. *Chem. - Eur. J.* **2012**, *18*, 16911−16921. (l) Berville, M.; Karmazin, L.; Wytko, J. A.; Weiss, J. *Chem. Commun.* **2015**, *51*, 15772−15775. (m) Wang, Y.; Frasconi, M.; Liu, W.-G.; Liu, Z.; Sarjeant, A. A.; Nassar, M. S.; Botros, Y. Y.; Goddard, W. A., III; Stoddart, J. F. *J. Am. Chem. Soc.* **2015**, *137*, 876−885.
(8) Hirayama, F. *J. Chem. Phys.* **1965**, *42*, 3163−3171.
(9) (a) Buck, A. T.; Paletta, J. T.; Khindurangala, S. A.; Beck, C. L.; Winter, A. H. *J. Am. Chem. Soc.* **2013**, *135*, 10594−10567. (b) Deronzier, A.; Galland, B.; Viera, E. *Nouv. J. Chim.* **1982**, *6*, 97−100.
(10) Kearney, A. M.; Vanderwal, C. D. *Angew. Chem., Int. Ed.* **2006**, *45*, 7803−7806.
(11) Gutmann, V. *Coord. Chem. Rev.* **1976**, *18*, 225−255.
(12) (a) Brandel, J.; Trabolsi, A.; Melin, F.; Elhabiri, M.; Weiss, J.; Albrecht-Gary, A.-M. *Inorg. Chem.* **2007**, *46*, 9534−9536. (b) Kadish, K. M.; Shiue, L. R.; Rhodes, R. K.; Bottomley, L. A. *Inorg. Chem.* **1981**, *20*, 1274−1277. (c) Weiss, J. *J. Inclusion Phenom. Mol. Recognit. Chem.* **2001**, *40*, 1−22.
(13) (a) Macias-Ruvalcaba, N. A.; Evans, D. H. *Chem. - Eur. J.* **2007**, *13*, 4386−4395. (b) Boulas, P. L.; Gomez-Kaifer, M.; Echegoyen, L. *Angew. Chem., Int. Ed.* **1998**, *37*, 216−247.
(14) Beletskaya, I.; Tyurin, V. S.; Tsivadze, A. Y.; Guilard, R.; Stern, C. *Chem. Rev.* **2009**, *109*, 1659−1713.
(15) te Velde, G.; Bickelhaupt, F. M.; Baerends, E. J.; Fonseca Guerra, C.; van Gisbergen, S. J. A.; Snijders, J. G.; Ziegler, T. *J. Comput. Chem.* **2001**, *22*, 931−967.
(16) Yang, Y.; Weaver, M. N.; Merz, K. M., Jr. *J. Phys. Chem. A* **2009**, *113*, 9843−9851.
(17) Tomasi, J.; Mennucci, B.; Cammi, R. *Chem. Rev.* **2005**, *105*, 2999−3094.
(18) (a) Johnson, E. R.; Keinan, S.; Mori-Sanchez, P.; Contreras-Garcıa, J.; Cohen, A. J.; Yang, W. *J. Am. Chem. Soc.* **2010**, *132*, 6498−6506. (b) Capdevila-Cortada, M.; Ribas-Arino, J.; Novoa, J. J. *J. Chem. Theory Comput.* **2014**, *10*, 650−658.
(19) The term stabilization refers to the fact that the peak potential corresponding to the reoxidation of the doubly reduced species gets shifted towards more positive values as the concentration in monomer increases. From an electrochemical point of view, V^0 being harder to oxidize implies that its stability domain increases or in other terms that V^0 has been stabilized.

DOI: 10.1021/jacs.6b09311
J. Am. Chem. Soc. 2016, 138, 15234−15242